Original Research

An increase in polyadenylation of histone isoforms, Hist1h2ah and Hist2h3c2, is governed by 3′-UTR in de-differentiated and undifferentiated hepatocyte

Tripti Verma[1,2], Abhiram Natu[1,2], Bharat Khade[1], Poonam Gera[3] and Sanjay Gupta[1,2]

[1]Epigenetics and Chromatin Biology Group, Gupta Lab, Cancer Research Institute, Advanced Centre for Treatment, Research and Education in Cancer, Tata Memorial Centre, Navi Mumbai 410210, India; [2]Homi Bhabha National Institute, Mumbai 400094, India; [3]Biorepository, Advanced Centre for Treatment, Research and Education in Cancer, Tata Memorial Centre, Navi Mumbai 410210, India
Corresponding author: Sanjay Gupta. Email: sgupta@actrec.gov.in

Impact statement

Environmental agents lead to diseases like cancer depending on the dose, duration of exposure, and individual's genetic background. Recent reports have shown that replication-dependent histone isoform transcripts are aberrantly polyadenylated instead of the standard stem-loop at 3′UTR with the degradation of stem-loop binding protein (SLBP) in response to heavy metals. This study indicates that SLBP loss and mRNA polyadenylation correlate with cellular stress *in vitro* and *in vivo* experiments. In coherence, hepatoblasts during embryonic development are hypoxic and have a low level of SLBP with enhanced polyadenylation of H2A and H3 isoforms. Moreover, persistent exposure to *N*-nitrosodiethylamine (NDEA), and enhanced histone mRNA polyadenylation, leads to increased histone protein levels driving the cells toward aneuploidy to maintain the DNA:histone ratio. The stress-associated imbalance in the level of SLBP and ARE (adenylate-uridylate-rich elements)-binding proteins, HuR, and BRF1 favors the increase in polyadenylated transcripts of histone isoforms, potentially one of the early events in carcinogenesis.

Abstract

Replication-dependent histones have a stem-loop structure at the 3′ end of messenger RNA (mRNA) and are stabilized by stem-loop binding protein (SLBP). Moreover, loss of SLBP and imbalance in the level of ARE (adenylate-uridylate-rich elements)-binding proteins, HuR, and BRF1 are associated with the polyadenylation of canonical histone mRNAs under different physiological conditions. Previous studies from the lab have shown increased protein levels of H2A1H and H3.2 in *N*-nitrosodiethylamine (NDEA)-induced hepatocellular carcinoma (HCC). In this study, we report that increase in the polyadenylation of histone mRNA contributes to increased levels of H2A1H and H3.2 in NDEA-induced HCC. The persistent exposure to carcinogen with polyadenylation of histone mRNA increases the total histone pool resulting in aneuploidy. The embryonic liver has also shown increased polyadenylated histone isoforms, Hist1h2ah and Hist2h3c2, primarily contributing to their increased protein levels. The increase in polyadenylation of histone mRNA in HCC and e15 are in coherence with the decrease in SLBP and BRF1 with an increase in HuR. Our studies in neoplastic CL38 cell line showed that direct stress on the cells induces downregulation of SLBP with enhanced histone isoform polyadenylation. Moreover, the polyadenylation is related to increase in activated MAP kinases, p38, ERK, and JNK in HCC liver tumor tissues and CL38 cells treated with arsenic. Our data suggest that SLBP degrades under stress, destabilizing the stem-loop, elongating histone isoforms mRNA with 3′ polyadenylated tail with increase of HuR and decrease of BRF1. Overall, our results indicate that SLBP may play an essential part in cell proliferation, at least in persistent exposure to stress, by mediating the stabilization of histone isoforms throughout the cell cycle.

Keywords: Histone isoforms, polyadenylation, carcinogenesis, stress, SLBP, ARE-binding proteins

***Experimental Biology and Medicine* 2023; 248: 948–958. DOI: 10.1177/15353702231160328**

Introduction

N-nitroso compounds (NOCs) and their precursors exist widely in the environment. Several occupational situations, foods, tobacco products, pharmaceutical drugs, and dietary components are known to form NOCs endogenously in the human body.[1,2] Moreover, *N*-nitrosodimethylamine (NDMA) and *N*-nitrosodiethylamine (NDEA) are categorized as etiological risk factors for human cancers, including liver, esophagus, stomach, and nasopharynx.[3] Animal studies have reported that persistent or chronic exposure to NDEA induces liver cancer due to metabolic activation of NDEA by cytochrome P450 2E1.[4] The carcinogenic effect of NDEA has potentially attributed to their DNA damaging and genotoxic properties. The genotoxic damages are critical in inducing chromosomal instability, changes in the ploidy status, and cancer development.[5] Moreover, recent studies have shown that increased levels of histone proteins are

linked to chromosome segregation defects and changes in ploidy status leading to genomic instability.[6,7]

During the S phase of the cell cycle, the chromatin-associated genomic DNA and histone proteins are completely duplicated. It is very well known that the expression of histone isoforms is regulated in a cell cycle–dependent manner which is synthesized and degraded during the S phase. The histone mRNA metabolism is regulated by SLBP at all the stages like pre-mRNA processing, histone synthesis, and degradation of the transcripts during the S phase of the cell cycle.[8]

Moreover, recent studies in cell lines have shown that the downregulation of SLBP under heavy metals, arsenic, nickel, and cadmium favors histone isoform polyadenylation, stability, and presence throughout the cell cycle.[9,10] Also, H3.1 polyA+ mRNA enhances the protein levels of H3.1 contributing to the displacement of histone H3.3 variant (coded by H3f3b) from active genomic regions. This leads to transcriptional deregulation, chromosome aneuploidy, and aberrations to potentially favor carcinogenesis.[11] In addition, the persistence of replication-dependent histones with polyadenylation at the 3′ end outside the S phase is now referred to as "histone stress," which has been shown to result in aneuploidy or whole genome duplication, which provides a proliferating advantage to cells.[7]

The polyadenylated canonical histone mRNA upon SLBP depletion under puromycin treatment and time-dependent exposure of UVC irradiation has been shown to provide accessibility to butyrate response factor 1, BRF1, or human antigen R, HuR. HuR and BRF1 bind to adenylate- and uridylate-rich cis-acting element (ARE) present in the 3′-UTR of replication-dependent histone isoforms resulting in either stability or degradation of polyadenylated histone transcripts, respectively.[12–15]

In rats, histone H2A isoforms comprise 12 different genes coding for nine proteins, and histone H3 isoforms have 2 genes coding for two proteins (http://www.actrec.gov.in/histome2/index.php). We previously demonstrated that persistent exposure to NDEA results in the development of hepatocellular carcinoma (HCC), with an increase in the histone H2A isoform, Hist1h2ah, and H3 isoform, Hist2h3c2. Moreover, the undifferentiated state of hepatocytes also has a higher histone H2A isoform, Hist1h2ah.[16,17] The altered histone H2A isoforms stoichiometry has been shown to affect nucleosome stability and physiological outcome.[18]

This study aimed to investigate whether increased levels of histone H2A and H3 isoforms in NDEA-induced liver cancer are due to the increase in the polyadenylated histone mRNA. Moreover, cancer-associated crosstalk among histone isoform-binding proteins, SLBP, BRF1, and HuR, with their downstream effects on histone fate, has not been explored. The data suggest that an NDEA-associated decrease of SLBP protein in crosstalk with BRF1 and HuR leads to a significant increase in polyadenylated transcripts of histone H2A and H3 isoforms in HCC tissue compared to normal liver. In coherence, the level of total histone pool increases, disturbing the DNA:histone stoichiometry which potentially leads to aneuploidy. Our results highlight genome instability induction due to polyadenylation of histones as a potential mechanism of cancer development in response to persistent exposure to hazardous environmental agents.

Materials and methods

Animal experiments

Institute Animal Ethics Committee duly approved the experimental proposals, ACTREC (08/2010 and 29/2011), and the experimental protocols were carried out as per Committee for the Purpose of Control and Supervision on Experiments on Animals (CPCSEA), India standards. The tissue samples stored at −80°C were used for experiments unless otherwise mentioned. Briefly, Sprague-Dawley rats (sp. *Rattus norvegicus; n* = 5) were given NDEA (100 ppm/g body weight) through drinking water for different periods to induce dysplastic nodules and HCC, as discussed earlier.[16] The methods used for liver tissue transplantation have been described previously.[19] As discussed, the embryonic liver and liver bud were excised from embryos on E15 from pregnant Sprague-Dawley rats. Hematoxylin and eosin staining of the collected liver tissues was carried out to confirm histopathology.[20] NDEA-induced HCC-derived rat neoplastic CL38 and preneoplastic CL44 cell lines were cultured in Eagle's minimum essential medium (MEM-6) and used in the study.

RNA isolation, cDNA synthesis, and quantitative polymerase chain reaction

Powdered tissue (100 mg) was used to isolate RNA using Agilent RNA isolation kit (Cat# 400800). The quality and quantity of RNA were confirmed by A_{260}/A_{280} and A_{260}/A_{230} absorbance using nanodrop followed by denaturing agarose gel. RNA (1 µg) was treated with DNase 1 and subjected to cDNA synthesis (RevertAid H-Minus first strand cDNA synthesis kit; Cat# K1632). The amplification was done with random hexamer primers for total mRNA and oligo dT primers for polyadenylated mRNA. The gene-specific rat primers mentioned in Table 1 were designed to determine the expression. Quantitative polymerase chain reaction (qPCR) was carried out by using Applied Biosystem's SYBR green master mix (Cat# 1725624) according to Qantstudio12Flex protocol. The expression levels are represented as a bar graph depicting the relative fold change of the genes normalized with the internal control. For statistical significance, an unpaired two-tailed Student's *t* test was applied, and graphs were made using GraphPad Prism 8.4.2 software.

Total lysate preparation and histone extraction

Total cell protein was extracted by resuspending 200 mg of powdered tissues in 2 mL lysis buffer (5 mM ethylenediaminetetraacetic acid [EDTA], 150 mM NaCl, 50 mM Tris, 10 mM EGTA [ethylene glycol tetraacetic acid], 25% Triton X-100, and proteinase inhibitor cocktail). The lysate was homogenized using a Kontron homogenizer and centrifuged at 4°C with 20,000 rpm for 20 min. Supernatant was collected, and protein estimation was carried out by Folin Lowry method.[21] The total lysate was prepared by adding loading dye followed by boiling for 10 min. For histone isolation, nuclei were extracted by sucrose density gradient centrifugation, followed by the acid extraction method.[22] The resolved histones on 18% gel were stained with Coomassie brilliant blue R-250 (CBBR) stain (0.1% CBBR w/v, 10% acetic acid, and 50% methanol in water) for 2–3 h and then destained with 50% methanol and 10% acetic acid in water.

Table 1. Gene-specific rat primer sequences for qPCR analysis.

S. no.	Gene	Forward (5′–3′)	Reverse (5′–3′)
1	Hist1h2ah	CTGTGCTGGAGTACCTGACG	TGTGGTGGCTCTCAGTCTTC
2	Hist1h2an	ACCTTACCTTTTCCACTTCCATCT	ATGCAGAAGCGTAGAGCCAA
3	Hist1h2ak	ACGAGGAGCTCAACAAGCTG	TGGTGGCTCTCGGTCTTCTT
4	Hist1h2af	GTGCACCGTCTGCTTTACAA	TGGCTCTCGGTCTTTTTGGG
5	Hist1h2ai	GGCGTTCTGCCAAACATCC	AAGAGCCTTTGGTGATCCCTG
6	Hist1h2ac	CACCACAAGGCCAAGGGAAA	GACTTGCGGTGCCATCTAGG
7	Hist2h2ab	CTAGGAGGAGTCACCATTGCC	TTTCCAGGCTTATGACTATCCGT
8	Hist1h3a	GGCTTTTCATCTTTTTCTTCCTACCATG	ACCGGTGGCCGGGGCACTTTTA
9	Hist2h3c2	ATGGCCCGTACAAAGCAG	AGGTTGGTGTCCTCGAACAG
10	H3f3b	TACCCTTCCAGAGGTTGGTG	GGGCATGATGGTGACTCTCT
11	Pan H4	GCATCTCCGGCCTCATCTAC	ACATCCATGGCAGTGACAGT
12	Cyclin D1	CGTGGCCACCTGGATGCTAGAG	TGCAGCAACTCCTCGGGGCGGAT
13	Cyclin B1	CCAAACCCCTGCTGAGATCG	CAGGCTCATCCAGTTCCACC
14	Cyclin E1	GACAGCTAGCGCGGTGTAG	GGACTTGGAACTCAGACCCG
15	PCNA	TCACAAAAGCCACTCCACTG	CATCTCAGAAGCGATCGTCA
16	RPS13	TGACGTCTGACGACGTGAAG	GGGCAAGGCCTTTGGACTTA

Western blotting and immunohistochemistry

Total lysates and histones prepared from tissues were separated on 12% and 18% SDS-PAGE (sodium dodecyl-sulfate polyacrylamide gel electrophoresis), respectively. Poly(vinylidene fluoride) (PVDF) membrane was used for probing the proteins with specific antibodies according to the manufacturer's protocol—PCNA (Abcam 1:3000), GAPDH (Cell Signaling 1:3000), SLBP (Sigma 1:3000), HuR (Invitrogen 1:5000), BRF1 (Invitrogen 1:2000), p38 (Santacruz 1:2000), p-P38 (Cell Signaling 1:2000), ERK (Cell Signaling 1:2000), p-ERK (Millipore 1:2000), JNK (Santacruz 1:2000), p-JNK (Cell Signaling 1:2000), Cyclin D1 (Cell Signaling 1: 1000), Cyclin E1 (Santacruz 1:1000), Cyclin B1 (Cell Signaling 1:1000), H3K56Ac (Abcam 1:4000), γ-H2AX (Millipore 1:4000), H4K16Ac (Millipore 1:8000), H3.3 (Sigma 1:5000), H3.2 (Millipore 1:4000), H3 (Millipore 1: 5000), H4 (Millipore 1:4000). The blots were developed using Clarity Max in Bio-Rad ChemiDoc machine. Immunohistochemistry staining was carried out using the Vectastain ABC kit (P6200) as described previously.[23] Briefly, 4-μm tissue sections were deparaffinized with xylene, and following rehydration with ethanol, antigen retrieval was carried out in a cooker using Tris/Sodium citrate buffer for each antibody. The anti-SLBP (Sigma 1:50), anti-HuR (Abcam 1:100), anti-BRF1 (Invitrogen 1:100), anti-PCNA (Abcam 1:100) were used for an overnight incubation at 4°C. The specific antigens were detected using diaminobenzidine (DAB; Sigma-D5537) and further counter-stained with hematoxylin before mounting.

Ultrapure nuclei isolation and flow cytometry

To isolate ultrapure nuclei, 3 g liver tissues were rinsed and homogenized in buffer A (60 mM KCl, 15 mM NaCl, 15 mM Tris-Cl pH 7.5, 0.5 mM EGTA, 2 mM EDTA, 0.15 mM 2-ME, 0.5 mM spermidine, and 0.15 mM spermine) with 0.34 M sucrose. The homogenate was centrifugated at 5000 rpm for 15 min; 4°C. The pellet was resuspended in 30 mL of fresh buffer A and layered on 10 mL of buffer A with 1.8 M sucrose, and centrifuged for 90 min at 26,000 rpm; 4°C in a swinging bucket rotor. The nuclear pellet was resuspended in 3 mL buffer A with 0.34 M sucrose and processed for flow cytometry. Nuclei were stained by vital dye and counted using hemocytometer; 10,000–20,000 nuclei used to measure DNA ploidy by flow cytometry were incubated with RNase A (10 mg/mL) and 2 μL Triton X-100 for 30 min, followed by propidium iodide (1 mg/mL) staining for 30 min as described.[24]

Transmission electron microscopy

Fixation of liver tissue pieces for microscopy was done using 3% glutaraldehyde followed by 1% osmium tetraoxide. Grids were contrasted by using alcoholic uranyl acetate and lead citrate for 60 and 30 s, respectively. The grids were observed; images were taken under a JEM 1400plus, JEOL (Japan) at 120 kV; and analysis was done using iTEM software.

Microarray data, Gene Ontology, and pathway analysis

Affymetrix RatGene10ST array platform was used for gene expression profile of two samples each of normal liver and HCC. The Affymetrix package in Bioconductor was used to perform the background expression value correction, data normalization, and probe summarization based on a robust multi-array average (RMA) algorithm. The gene expression matrix was then subjected to identify differentially expressed genes (DEGs) between the two groups in linear models for the microarray data (limma) package. The cut-off values for the DEGs identification were FDR (false discovery rate) < 0.05 and log2 fold change $> \pm 1.5$. A volcano plot was generated in R (4.0) using the plot function.

Gene Ontology (GO) KEGG (Kyoto Encyclopedia of Genes and Genomes) pathway analysis was used to understand the functional roles of DEGs. For functional annotation, the DEGs were subjected to DAVID tool. FDR < 0.05 in both GO and KEGG analyses were considered as the threshold for significant enrichment. The data obtained for functional analysis was represented by converting FDR values into $-\log_{10}$ (FDR) in the bar graph.

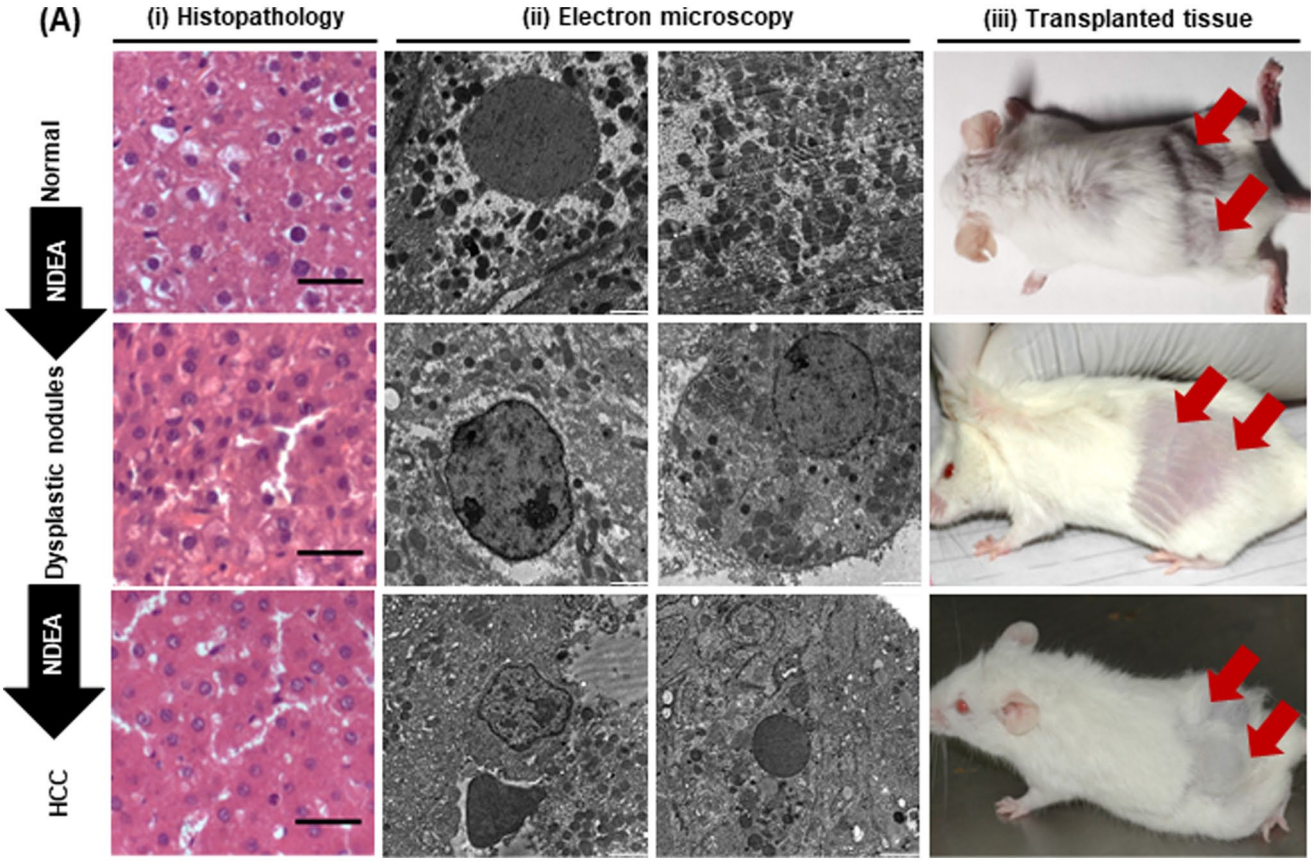

Figure 1. Characterization of NDEA-induced tumors. (A) (i) Representative images of hematoxylin and eosin (H&E) stained (scale bars represent 1 μm) and (ii) tissue sections processed for electron microscopy of normal, dysplastic nodules, and hepatocellular carcinoma induced by NDEA treatment. Scale bars represent 2000 nm. (iii) The liver tissues of normal, 45-day, and 105-day NDEA-treated animals were implanted in NOD-SCID (non-obese diabetic/severe combined immunodeficiency) mice to study transformation potential.

Statistical analysis

Statistical analyses were carried out with GraphPad Prism 8.4.2 software. All experimental results are represented as mean ± standard deviation. The mean of groups was analyzed by an unpaired Student's *t* test. The *P* value less than 0.05 was taken for statistical significance.

Results

Characterization of NDEA-induced tumors

Histopathological analysis of normal liver showed hepatic architecture with perfectly polygonal cells, normal parenchyma, and granulated cytoplasm. After 45 days of NDEA treatment, the liver tissues showed dysplastic behavior with focal lesion formation, serosis, and vacuolar degeneration. Aggregated hepatocellular alteration with degenerative nuclear changes, enlarged foci/nodules, and inflammation implied neoplastic changes in HCC tissue samples (Figure 1(A, i)).

In addition, electron microscopic analysis displayed marked ultrastructural changes progressing from normal liver to HCC tumor tissues. The normal group depicted regular cell morphology, nuclear architecture, nuclear to cytoplasmic ratio, tight cellular junction, ample cytoplasmic organelles constituting well-organized mitochondria, endoplasmic reticulum, and Golgi complexes. The dysplastic nodules showed hepatocytes with the altered endoplasmic reticulum, swollen mitochondria, loose membrane integrity, and uneven nuclear architecture with highly dense areas suggestive of a heterochromatin state on the nuclear lamina. HCC tissues showed distinct cell shrinkage with disordered nuclear shape and cytoplasm sparse, resulting in a significant increase in nuclear to cytoplasmic ratio and heterochromatin state. Moreover, a significant decrease in mitochondrial number and loss of the rough endoplasmic reticulum layered structure was observed (Figure 1(A, ii)). The transformation potential of HCC was confirmed by implantation of 3-mm^2 liver tissue samples from normal, dysplastic, and HCC in NOD-SCID (non-obese diabetic/severe combined immunodeficiency) mice. The data showed the development of xenografts only with HCC liver tissue samples (Figure 1(A, iii)).

Gene-expression profiling of carcinogen-induced liver tumor

Genome-wide expression analysis was carried out in normal and HCC liver tissue, and DEGs were identified with a cut-off value of FDR < 0.05, and log2 fold change $> \pm 1.5$ was represented as volcano plot (Figure 2(A, i)), and to understand their functional significance, GO pathway analysis was carried out. The differentially upregulated pathways

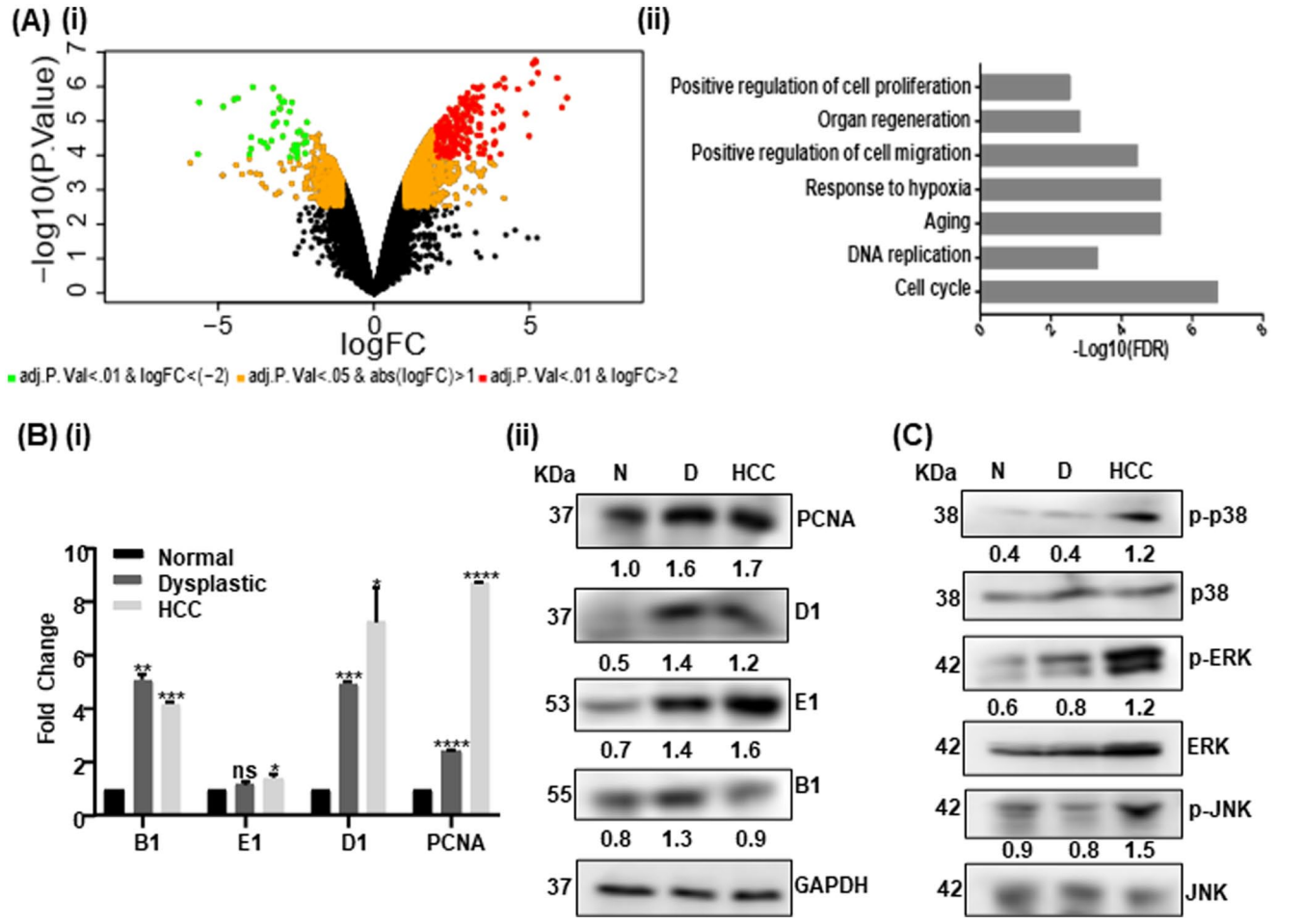

Figure 2. Gene-expression profiling and validation of proteins associated with carcinogen-induced liver tumor (A) (i) Volcano plot representation of differentially expressed genes among normal and HCC liver tissue with cut-off values FDR < 0.05 and log2 fold change $> \pm 1.5$. Red and green dots signify the upregulated and downregulated genes, respectively. (ii) Bar graph representation of most significant upregulated pathways in HCC compared to normal. (B) (i) qPCR analysis depicting the fold change in mRNA expression of cyclin B1, E1, D1, and PCNA in dysplastic and HCC tissues as compared to normal is represented as a bar graph. RPS13 was used as an internal control. (ii) Western blotting data showing the protein levels of cyclin D1, E1, B1, and PCNA in normal, dysplastic, and HCC tissues. GAPDH was used as a loading control and used for the normalization of cyclins. (C) The total and phosphorylated ERK, p38, and JNK levels were studied by western blotting in normal, dysplastic, and HCC tissues. The level of activated MAP kinases was normalized with respective total levels of the kinases. Student's unpaired *t* test ($P < 0.05$ denotes *, $P < 0.01$ denotes **, $P < 0.001$ denotes ***, and $P < 0.0001$ denotes ****) was carried out for statistical analysis of the obtained data. N: normal liver; D: dysplastic nodules; HCC: hepatocellular carcinoma.

include cell proliferation, cell migration, DNA replication, and cell cycle pathways (Figure 2(A, ii)).

A key question is whether the upregulated pathways at the mRNA level cause increase in the steady-state levels of specific proteins; therefore, the mRNA and protein levels of PCNA, cyclin D1, E1, and B1 were studied. The transcripts of cyclin D1, B1, and PCNA were significantly elevated in dysplastic nodules and HCC, whereas the E1 mRNA was significantly increased in HCC only (Figure 2(B, i)). The western blot data showed that treatment with nitrosamine significantly enhances the protein levels of cyclin D1, E1, and PCNA. In contrast, the B1 protein level does not change considerably in dysplastic nodules and HCC samples compared to normal tissues with GAPDH as an internal control (Figure 2(B, ii)). Earlier reports have shown the stabilization of cyclin B1 mRNA by HuR.[25] In coherence, IHC-PCNA showed increased nuclear staining intensity in dysplastic nodules and HCC (Supplemental Figure S1-A). Furthermore, western blot studies were carried out to delineate whether the persistent treatment with NDEA affects MAPK (mitogen-activated protein kinase) signaling pathways. The data showed phosphorylated form of p38, ERK, and JNK increases at the protein levels without significant change in the total level of MAP kinases, p38, ERK1/2, and JNK in HCC compared to normal liver.

Histone H2A and H3 isoforms undergo polyadenylation in NDEA-induced liver cancer

The increased proliferation will require higher levels of histone proteins for chromatin reorganization during DNA replication. Therefore, profiling of total and polyadenylated histone H2A and H3 isoform mRNA was carried out. Interestingly, histone H2A isoform Hist1h2ah showed a concomitant increase in total mRNA and polyadenylated mRNA levels in dysplastic and HCC tissues compared to normal (Figure 3(A)). Increased protein levels of H2A1H have already been reported in NDEA-induced HCC.[16] Moreover, other H2A isoforms, Hist1h2an, Hist1h2ak, Hist1h2af, Hist1h2ai, Hist1h2ac, Hist2h2ab, have also shown a similar

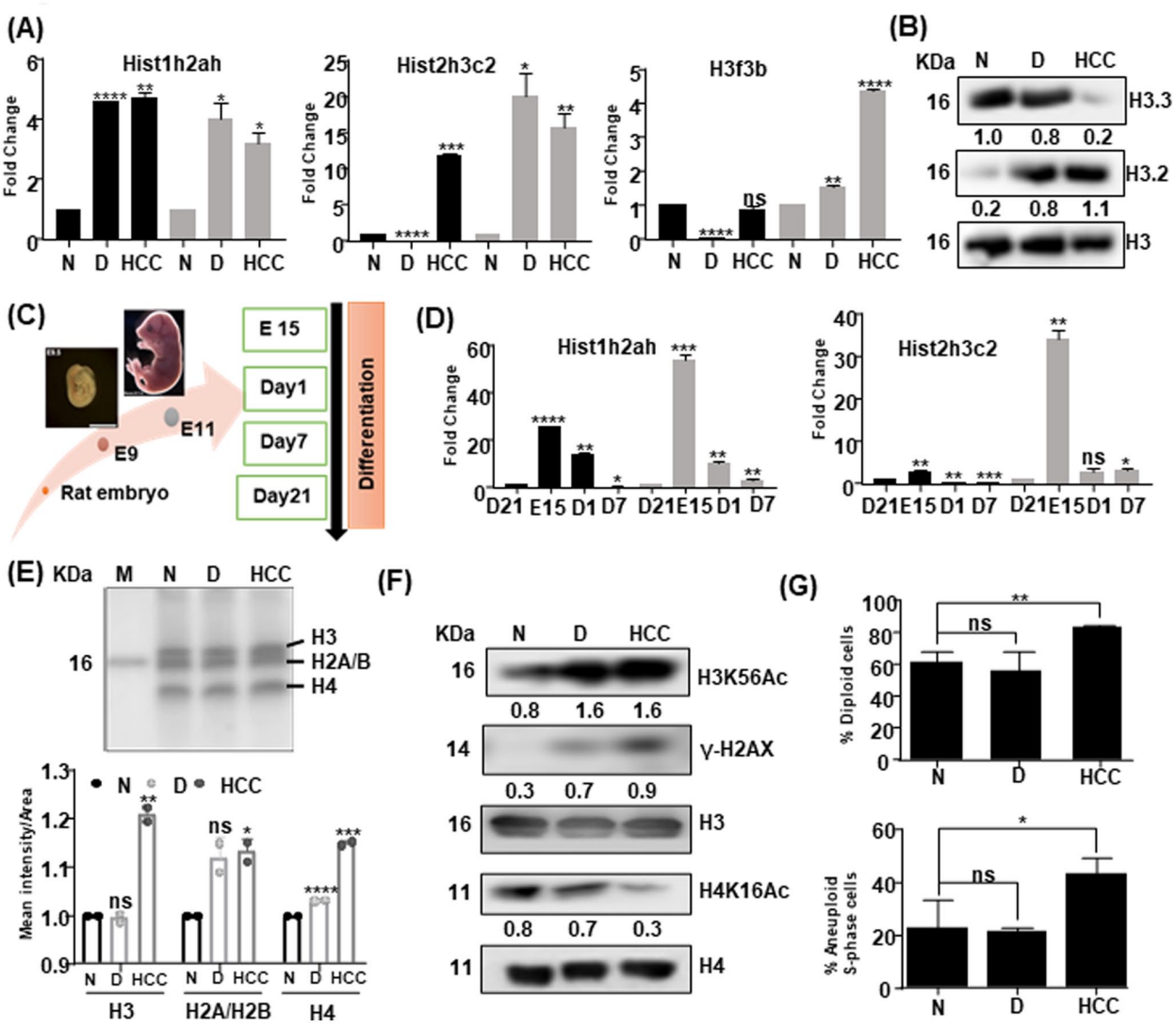

Figure 3. Histone H2A and H3 isoforms undergo polyadenylation in NDEA-induced liver cancer. (A) Bar graphs represent relative fold change of total and polyadenylated levels of rat histone H2A isoform, that is, Hist1h2ah and rat histone H3 isoforms, that is, Hist2h3c2 and H3f3b. Total H4 was used as an internal control. (B) The protein levels of H3.2 and H3.3 was studied to correlate with the altered levels of polyadenylated mRNA. Total H3 was used as a loading control. (C) Schematic representation of liver differentiation model depicting the development of embryonic hepatoblast (E15) to the liver (D21). (D) Bar graphs representing relative fold change of total and polyadenylated levels of histone H2A isoforms, Hist1h2ah, and Hist2h3c2 in embryonic hepatoblast tissue compared to D1, D7, and D21 liver tissue samples. RPS13 was used as an internal control. (E) Coomassie-stained gel exhibiting total core histones among normal, dysplastic, and HCC histones isolated from an equal number of ultrapure nuclei. The mean intensity of respective histone bands is plotted as a bar graph. (F) Western blot analysis of epigenetic genomic instability markers, that is, gain of H3K56Ac, γH2AX, and loss of H4K16Ac during cancer progression. Total H3 and H4 were used as a loading control. (G) Bar graph representation of flow cytometric analysis of ultrapure nuclei depicting % diploid and % aneuploid cells in normal, dysplastic, and HCC liver tissues ($n = 3$). Student's unpaired t test ($P < 0.05$ denotes *, $P < 0.01$ denotes **, $P < 0.001$ denotes ***, and $P < 0.0001$ denotes ****) was carried out for statistical analysis of the obtained data. Black bars represent total mRNA levels, and gray bars represent polyadenylated mRNA levels. N: normal liver; D: dysplastic nodules; HCC: hepatocellular carcinoma; E15: embryonic hepatoblast; D1: day 1 (day of birth); D7: day 7; D21: normal liver.

results (Supplemental Figure S2-A). However, histone H3 isoform Hist2h3c2 showed an increase in their total mRNA levels in HCC tissues; nevertheless, accumulation of polyadenylated transcripts in both dysplastic and HCC tissues was observed. Histone H3 variant H3f3b was a positive control (Figure 3(A)). Western blot analysis showed that the level of H3.3 protein decreases in tumor tissue samples. Moreover, H3.2 protein showed upregulation in cancer, suggesting that increased polyadenylation levels of Hist2h3c2 are increasing the turnover of H3.2 protein (Figure 3(B)).

Whether the observed changes are specific to de-differentiation, histone levels were profiled for the total and polyadenylated mRNA in undifferentiated embryonic liver tissues (e15). (Figure 3(C)) (Figure S1-B). Strikingly, Hist1h2ah and Hist2h3c2 isoforms showed a significant increase of both total and polyadenylated mRNA in e15 with a sequential decrease in the order of e15 > D1 > D7 and D21 (Figure 3(D)). Previous reports have shown the association of H2A1H with the undifferentiated state of hepatocytes.[17] Together, the data suggest that mRNA transcripts of total histone and polyadenylated histone were increased for all the histone isoform genes; however, an increase of histone isoform levels is an outcome of enhanced polyadenylated transcripts in de-differentiated, HCC and undifferentiated, e15 liver tissues.

The increase in the histone mRNA may influence the total histone protein level. Histones isolated from equal number of ultrapure nuclei of normal, dysplastic, and HCC tissue were resolved, stained with Coomassie R250, and the mean

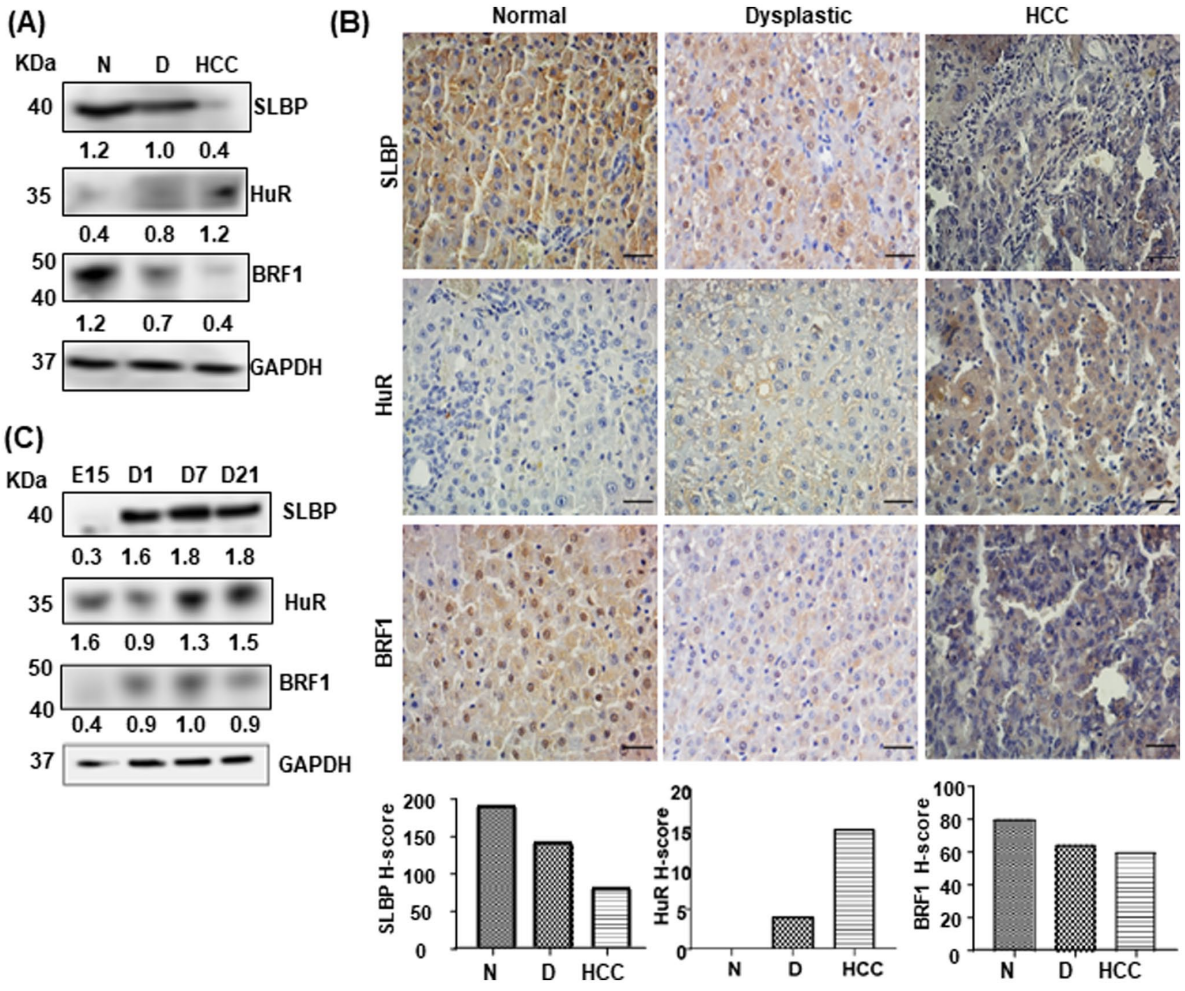

Figure 4. Histone isoform polyadenylation with SLBP downregulation and crosstalk with HuR and BRF1 in NDEA-induced HCC model. (A) Western blot analysis and (B) representative IHC images (magnification 40×) for SLBP, HuR, and BRF1 in normal, dysplastic, and HCC tissue samples. Scale bars represent 1 μm. H-score for IHC was calculated based on intensity (0–3 equivalent to none, weak, moderate, and strong) and proportion of the proteins, and the values obtained were plotted as a bar graph. (C) Protein levels of SLBP, BRF1, and HuR in embryonic hepatoblast, postnatal D1, D7, and D21 liver tissues were studied by western blot. GAPDH was used as a loading control. N: normal liver; D: dysplastic nodules; HCC: hepatocellular carcinoma; E15: embryonic hepatoblast; D1: day 1 (day of birth); D7: day 7; D21: normal liver.

intensity of the respective histone bands was plotted as a bar graph (Figure 3(E)). The data showed an increase in the level of core histones in HCC compared to normal and dysplastic tissue samples. This finding suggests that the increase in total histone protein levels is a consequence of increased polyadenylation of histone isoforms.

Moreover, epigenetic markers of genomic instability showed a gain of H3K56Ac and γH2AX and loss of H4K16Ac, concluding that genomic instability increased in NDEA-induced HCC (Figure 3(F)). In coherence, HCC tissues showed a significant increase in percent diploid and S-phase aneuploid cells rendering genomic instability with no substantial change in dysplastic tissues, as also observed in total histone levels earlier (Figure 3(G)). These findings suggest that an increase in the DNA content as the tumor progresses must demand the fulfillment of ample histone synthesis to maintain the DNA: histone stoichiometry, bringing the involvement of epigenetic factors into the limelight. Therefore, on short-term exposure to a carcinogen, NDEA leads to dysplastic changes and the potential to proliferate; however, they lack certain factors or stimuli that keep them from attaining tumorigenic fate. However, persistent exposure to NDEA promotes the development of HCC.

Histone isoform polyadenylation with SLBP downregulation and crosstalk with HuR and BRF1 in NDEA-induced HCC

The differential expression of HuR and BRF1 under normal physiological conditions has already been reported.[15,26] However, to investigate whether the SLBP, HuR, and BRF1 protein levels during cancer progression correlate with the stability of polyadenylated histone, western blotting and IHC were performed. The data showed a sequential decrease in SLBP and BRF1 with an increase in HuR protein expression with the development of HCC in response to NDEA treatment. (Figure 4(A) and (B)). H-scoring for IHC was done on the basis of intensity and proportion for the protein of interest in the tissue section. SLBP and BRF1 showed positive nuclear and cytoplasmic staining in normal liver tissues with a sequential decrease in dysplastic and HCC tissue. In contrast, HuR showed a predominant presence in the cytoplasm

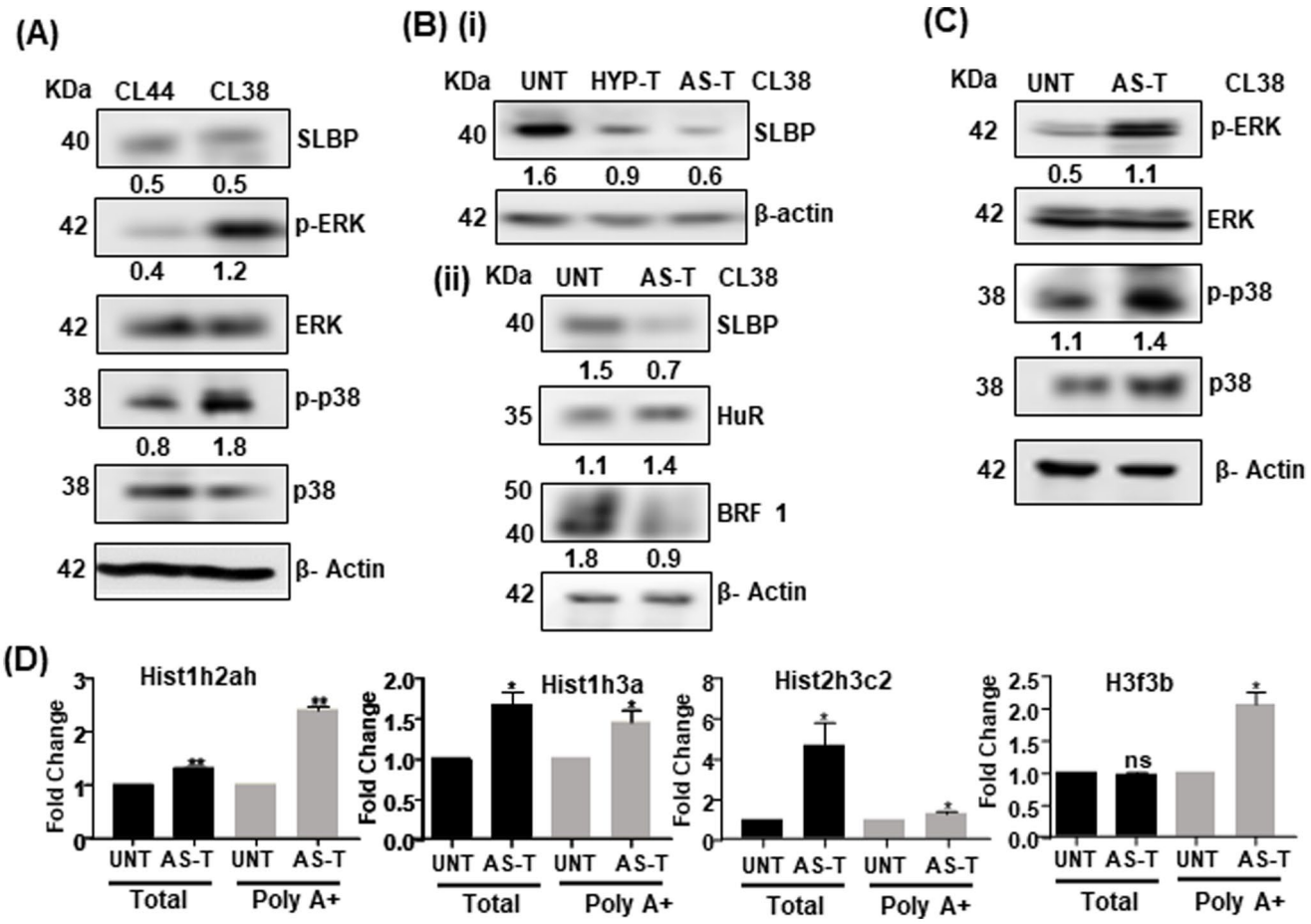

Figure 5. Association of stress with SLBP downregulation and histone polyadenylation. (A) Protein levels of SLBP, p-ERK, and p-p38 in pre-neoplastic CL44 and neoplastic CL38 cell lines are depicted by western blotting. Total ERK and p-38 levels are used to normalize the active form of respective MAP kinases. β-actin was used as an internal loading control. (B) (i) Protein levels of SLBP in CL38 untreated (UNT), exposed to 1% hypoxia (HYP-T), and 0.5 ng/μL arsenic-treated (AS-T) cells. β-actin was used to normalize the levels of respective proteins. (ii) Protein levels of SLBP, HuR, and BRF1 in CL38 untreated (UNT) and 0.5 ng/μL arsenic-treated cells (AS-T) were studied by western blotting. (C) p-ERK and p-p38 levels in arsenic-treated (0.5 ng/μL) cells (AS-T) compared to CL38 untreated cells (UNT) depicted by western blot. Total ERK and p-38 levels were used for the normalization of respective MAP kinases. β-actin was used as an internal loading control. (D) Bar graphs representing relative fold change of total and polyadenylated levels of histone H2A isoform Hist1h2ah, H3 isoforms Hist1h3a and Hist2h3c2, H3 variant H3f3b in CL38 untreated cells (UNT), and arsenic-treated (0.5 ng/μL) cells (AS-T). RPS13 was used as an internal control. Student's unpaired *t* test ($P < 0.05$ denotes *, $P < 0.01$ denotes **, $P < 0.001$ denotes ***, and $P < 0.0001$ denotes ****) was carried out for statistical analysis of the obtained data. Black bars represent total mRNA levels, and gray bars represent polyadenylated mRNA levels. UNT: untreated; HYP-T: hypoxia treated; AS-T: arsenic-treated.

and was significantly higher in HCC tissue than in the normal. The subsequent depletion of SLBP from dysplastic to HCC tissue leads to aberrant processing of histone isoforms, which allows the recruitment of HuR, potentially stabilizing the histone mRNA.

In our previous results, embryonic liver tissue (e15) showed enhanced polyadenylation of histone mRNA. Interestingly, a decrease in SLBP and BRF1 with increased levels of HuR was observed in undifferentiated embryonic e15 liver tissue compared to differentiated liver tissues. (Figure 4(C)). Collectively, over-expressed HuR helps in stabilization of polyadenylated histone mRNAs by binding to ARE element.

SLBP downregulation and histone polyadenylation are associated with stress

In vitro studies with NDEA-derived rat neoplastic cell line, CL38, and pre-neoplastic cell line, CL44, showed no significant alteration in the level of polyadenylated mRNA for Hist1h2ah, Hist2h3c2, and SLBP protein among the cell lines. These observations were not in coherence with HCC tumor tissues data. Earlier studies have reported the importance of MAP kinases in different stages of cancer development.[27] Therefore, we studied the levels of active MAP kinases, and the data showed that p-ERK and p-p38 levels were increased in CL38 neoplastic cells, as expected, compared to pre-neoplastic cells (Figure 5(A), Supplemental Figure S2-D).

The cells in *in vitro* culture are not under the stress of nutrition and oxygen concentration and may behave differently from cells *in vivo*. Regarding stress on the level of SLBP protein, CL38 cells were treated with hypoxia (1%) and arsenic at a low dose (0.5 ng/μL) for 48 h. The treated cells showed significant depletion of SLBP in hypoxia and arsenic-treated CL38 cells. Furthermore, arsenic-treated cells showed a decrease in BRF1 with a slight increase in HuR protein compared to untreated CL38 cells (Figure 5(B, i and ii)). Moreover, the stress-associated upregulation of p-ERK and p-p38 was observed upon arsenic treatment to CL38 cells (Figure 5(C)). Therefore, stress factor plays a critical role in defining the fate of SLBP protein.

Moreover, the real-time PCR analysis showed an increase in total and polyadenylated mRNA levels of histone isoforms Hist1h2ah, Hist1h3a, and Hist2h3c2 in arsenic-treated cells compared to untreated CL38 cells. H3f3b variant was used as a positive control. Overall, a stress-associated decrease in the SLBP protein favors the increase in the histone isoforms polyadenylation.

Discussion

The replication-dependent histone isoforms are transcribed during S phase and synchronized with DNA replication for incorporation into chromatin. The SLBP protein stabilizes the stem-loop at 3′UTR and is involved in processing histone mRNA.[28] Our earlier studies have shown increased levels of histone protein H2A1H in NDEA-induced liver cancer and embryonic hepatoblast (e15).[16,17] Moreover, a recent study has also shown an increase of H3.2 at protein and total mRNA levels in HCC.[29] The present *in vivo* studies define that increased polyadenylation of Hist1h2ah and Hist2h3c2 mRNA significantly contributes to the enhanced levels of their total mRNA. The mRNA alteration is consistent with a decreased SLBP protein level in HCC and e15 hepatoblast. The observed increase in polyadenylated histone isoforms in e15 hepatoblast is potentially due to the degradation of maternally supplied SLBP during embryogenesis.[30] Previous reports have shown that depletion of SLBP promotes the accumulation of polyadenylated H3.1.[31]

Moreover, Chen *et al.*[11] have also shown that over-expression of polyadenylated H3.1 and replacement of H3.3 variant, with SLBP knockdown, significantly enhanced both anchorage-independent cell growth and increase in number of colonies leading to cellular transformation. However, nucleosomes are constituted by two copies each of core histones. In this study, the polyadenylation of other histone isoforms of H2A and H3, that is, Hist1h2ah and Hist2h3c2, respectively, is observed. Therefore, the mechanism of histone variant H3.3 getting replaced by polyadenylated isoform H3.1 as mentioned in earlier reports could hold true with any other histone isoform as well, as shown in our present study for histone isoforms Hist1h2ah and Hist2h3c2.

However, we now show that SLBP protein levels are significantly low in HCC or embryonic hepatoblast tissues, suggesting that SLBP indeed decreases under stress conditions. The hypoxic stress with $O2 < 2\%$ during early embryogenesis might promote SLBP degradation. Earlier study has also shown that alterations in epigenetic mechanisms due to stress-associated proteins mediate specific lineages during development from fruit flies to mammals.[32] In normal cell proliferation during liver regeneration, the levels of SLBP protein do not change (data not shown). These data suggest the association of stress with the levels of SLBP protein.

Moreover, *in vitro* studies with cancer cell lines have shown no significant change in the level of SLBP, for which the potential reason could be a lack of stress factors, that is, insufficient oxygen and nutrient supply, experienced by solid tumor cancer cells *in vivo* which are not recapitulated in *in vitro* conditions. However, an increase in the p-ERK and p-p38 was observed pertaining to the neoplastic nature of the CL38 cell line. Interestingly, arsenic exposure to CL38 cells showed a significant increase in p-ERK and p-p38 levels suggesting that direct stress to the cells decreased SLBP levels with a substantial increase in polyadenylated histone H2A and H3 isoforms. Moreover, our data also showed an increase in the MAP kinase pathway, which associates with proliferation in tumor tissues, further indicating the stress-associated change to the cancer phenotype, HCC. Arsenic, nickel, and cadmium-induced oxidative stress have been shown to deplete SLBP, an essential parameter for polyadenylation of canonical histone mRNAs.[9,33] Brocato *et al.*[10] have demonstrated that a decrease in SLBP after arsenic exposure is due to DNA methylation of the SLBP promoter and increased proteasomal degradation. It will be interesting to decipher whether SLBP gets demethylated in cancer cell lines in the presence of active MAP kinases. Therefore, stress deflects the typical trajectories of development, growth, and de-differentiation downward.

The stability of polyadenylated histone isoform mRNA is essential for the post-transcriptional regulation of gene expression. The stability and degradation of polyadenylated mRNA of histone isoforms are regulated by the RNA-binding proteins, HuR and BRF1, under stress conditions like puromycin treatment and UVC irradiation, respectively. These proteins bind to adenylate-uridylate-rich element (ARE) downstream of the stem-loop in 3′UTR mRNA of canonical histones.[12,13] The present data have shown an inverse relationship between the level of SLBP and BRF1 with the levels of HuR and increased polyadenylated histone mRNA tails in HCC tissues, cancer cells treated with arsenic, and embryonic e15 hepatoblast. Here, the increase in HuR levels, a protein known to stabilize and decrease in BRF1, a protein known to degrade the polyadenylated histones, favors the increase in histone isoforms mRNA with a polyadenylated tail. Earlier studies from human tissues have also suggested that HuR and AUF1 are implicated in the process of liver cancer development.[26]

p38, ERK2, and downstream MK2 have been implicated in tristetraprolin (TTP) phosphorylation, inhibiting its ARE-binding activity.[34] Also, Wilson *et al.*[35,36] have shown that the alteration in the phosphorylation of BRF1 or AUF1 in response to stress leads to changes in the ARE interacting complex. In such conditions, the stabilizing factor, HuR, binds to ARE element and stabilizes the mRNA. Thus, the imbalance in the levels of ARE-binding proteins, stabilizing (HuR), and destabilizing (BRF1) factors will be important to maintain the level of polyadenylated histone isoforms.

The polyadenylated histone isoforms increase the pool of histone proteins, potentially contributing to genomic instability to reprogram the gene expression for the survival of cancer cells. Several studies have also shown that histone stress induces whole genome doublings and polyploidy in *Saccharomyces cerevisiae*. The studies have also shown that histone metabolism gets altered during stress conditions, leading to a persistent presence of histone isoforms throughout the cell cycle, resulting in the delayed nuclear division that triggers polyploidy.[37–39] Interestingly, we have shown that an increase in total levels of histone proteins in HCC is concomitant with an increase in diploid and aneuploidy S-phase cells. Interestingly, levels of cell proliferation markers showed upregulation in both dysplastic and HCC, and

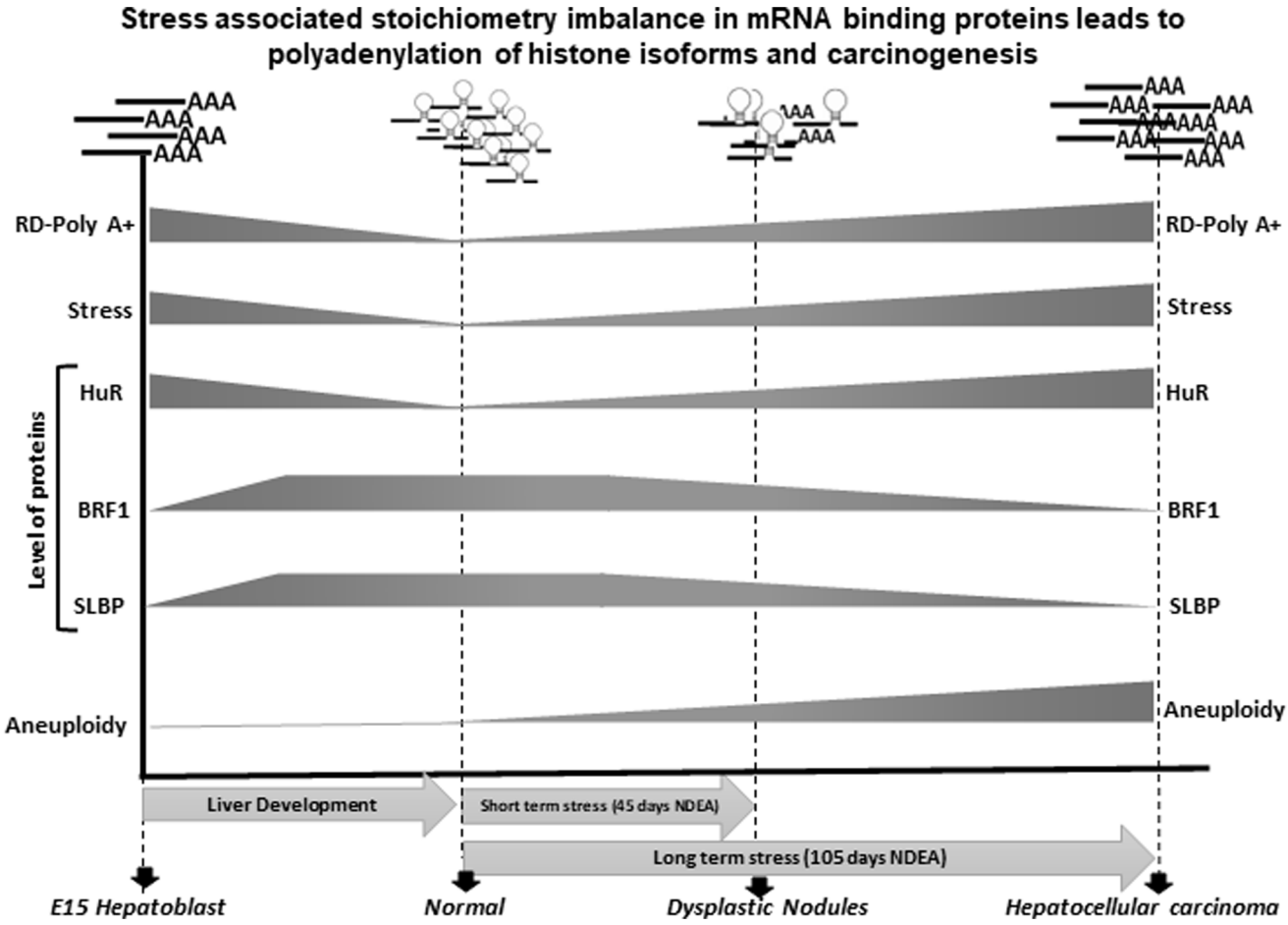

Figure 6. Model depicting the stress is associated with a stoichiometric imbalance in histone mRNA-binding proteins, SLBP, BRF1, and HuR, leading to polyadenylation of histone H2A and H3 isoforms in early embryonic hepatoblast and NDEA-induced HCC. The persistent stress increases the levels of stable polyadenylated histone mRNA and the total pool of histone protein. In consequence, the DNA content increases to maintain the ratio of DNA to histone. This increase of DNA content is in coherence with gradual increase in the aneuploidy in hepatocellular carcinoma.

aneuploidy was significantly observed only in HCC tumor tissues indicating that cancer development is governed by epigenetic priming of initiator cells, which lies in a dormant state until promoted by persistent exposure to environmental stimuli.[40]

In summary, continuous exposure to the carcinogen or stress-associated decrease in SLBP favoring histone isoform polyadenylation replacing histone variants might be one of the initial events that prompts the establishment of "initiated cells" in the carcinogenesis process. In parallel, the altered levels of HuR and BRF1 protein govern the fate of polyadenylated mRNA of histone isoforms (Figure 6). Future research should emphasis on understanding the extent, dose, or persistence of stress-inducing agents, physical, biological, and chemical, with altered stability of histone isoforms and phenotypic outcomes that affect prenatal and postnatal life.

AUTHORS' CONTRIBUTIONS

TV performed the major experiments. AN analyzed the microarray data. BK contributed in animal experiments. PG contributed to the analysis of H&E stained and IHC slides. SG, TV, and AN wrote the manuscript. All authors approved the manuscript.

ACKNOWLEDGEMENTS

Thanks to Dr H. M. Rabes (University of Munich, Germany) for providing authors with the CL44 and CL38 cell lines for research purposes.

DECLARATION OF CONFLICTING INTERESTS

The author(s) declared no potential conflicts of interest with respect to the research, authorship, and/or publication of this article.

FUNDING

The author(s) disclosed receipt of the following financial support for the research, authorship, and/or publication of this article: The financial support for the research was provided by the Advanced Centre for Treatment Research and Education in Cancer (grant number 42). TV and AN thank Advanced Centre for Treatment Research and Education in Cancer (ACTREC) for fellowship.

ORCID ID

Sanjay Gupta https://orcid.org/0000-0002-1209-189X

SUPPLEMENTAL MATERIAL

Supplemental material for this article is available online.

REFERENCES

1. Tricker AR. N-nitroso compounds and man: sources of exposure, endogenous formation and occurrence in body fluids. *Eur J Cancer Prev* 1997;**6**:226–68
2. Dubrow R, Darefsky AS, Park Y, Mayne ST, Moore SC, Kilfoy B, Cross AJ, Sinha R, Hollenbeck AR, Schatzkin A, Ward MH. Dietary components related to N-nitroso compound formation: a prospective study of adult glioma. *Cancer Epidemiol Biomarkers Prev* 2010;**19**:1709–22
3. Tricker AR, Preussmann R. Carcinogenic N-nitrosamines in the diet: occurrence, formation, mechanisms and carcinogenic potential. *Mutat Res* 1991;**259**:277–89
4. Mukherjee D, Ahmad R. Dose-dependent effect of N′-Nitrosodiethylamine on hepatic architecture, RBC rheology and polypeptide repertoire in Wistar rats. *Interdiscip Toxicol* 2015;**8**:17
5. Hanahan D. Hallmarks of cancer: new dimensions. *Cancer Discov* 2022;**12**:31–46
6. Duesberg P, Fabarius A, Hehlmann R. Aneuploidy, the primary cause of the multilateral genomic instability of neoplastic and preneoplastic cells. *IUBMB Life* 2004;**56**:65–81
7. Miles DM, Desdouets C, Géli V. Histone stress: an unexplored source of chromosomal instability in cancer. *Curr Genet* 2019;**65**:1081–8
8. Marzluff WF, Wagner EJ, Duronio RJ. Metabolism and regulation of canonical histone mRNAs: life without a poly(A) tail. *Nat Rev Genet* 2008;**9**:843–54
9. Jordan A, Zhang X, Li J, Laulicht-Glick F, Sun H, Costa M. Nickel and cadmium-induced SLBP depletion: a potential pathway to metal mediated cellular transformation. *PLoS ONE* 2017;**12**:e0173624
10. Brocato J, Chen D, Liu J, Fang L, Jin C, Costa M. A potential new mechanism of arsenic carcinogenesis: depletion of stem-loop binding protein and increase in polyadenylated canonical histone H3.1 mRNA. *Biol Trace Elem Res* 2015;**166**:72–81
11. Chen D, Chen QY, Wang Z, Zhu Y, Kluz T, Tan W, Li J, Wu F, Fang L, Zhang X, He R, Shen S, Sun H, Zang C, Jin C, Costa M. Polyadenylation of histone H3.1 mRNA promotes cell transformation by displacing H3.3 from gene regulatory elements. *iScience* 2020;**23**:101518
12. Ryu I, Park Y, Seo JW, Park OH, Ha H, Nam JW, Kim YK. HuR stabilizes a polyadenylated form of replication-dependent histone mRNAs under stress conditions. *FASEB J* 2019;**33**:2680–93
13. Ryu I, Kim YK. AU-rich element-mediated mRNA decay via the butyrate response factor 1 controls cellular levels of polyadenylated replication-dependent histone mRNAs. *J Biol Chem* 2019;**294**:7558–65
14. Mukherjee N, Corcoran DL, Nusbaum JD, Reid DW, Georgiev S, Hafner M, Ascano MJ, Tuschl T, Ohler U, Keene JD. Integrative regulatory mapping indicates that the RNA-binding protein HuR couples pre-mRNA processing and mRNA stability. *Mol Cell* 2011;**43**:327–39
15. Raineri I, Wegmueller D, Gross B, Certa U, Moroni C. Roles of AUF1 isoforms, HuR and BRF1 in ARE-dependent mRNA turnover studied by RNA interference. *Nucleic Acids Res* 2004;**32**:1279–88
16. Khare SP, Sharma A, Deodhar KK, Gupta S. Overexpression of histone variant H2A.1 and cellular transformation are related in N-nitrosodiethylamine-induced sequential hepatocarcinogenesis. *Exp Biol Med* 2011;**236**:30–5
17. Tyagi M, Khade B, Khan SA, Ingle A, Gupta S. Expression of histone variant, H2A.1 is associated with the undifferentiated state of hepatocyte. *Exp Biol Med* 2014;**239**:1335–9
18. Bhattacharya S, Reddy D, Jani V, Gadewal N, Shah S, Reddy R, Bose K, Sonavane U, Joshi R, Smoot D, Ashktorab H, Gupta S. Histone isoform H2A1H promotes attainment of distinct physiological states by altering chromatin dynamics. *Epigenetics Chromatin* 2017;**10**:48
19. Bhattacharya S, Reddy D, Ingle A, Khade B, Gupta S. Histone H2A mono-ubiquitination and cellular transformation are inversely related in N-nitrosodiethylamine-induced hepatocellular carcinoma. *Exp Biol Med* 2016;**241**:1739–44
20. Shah SG, Rashid M, Verma T, Ludbe M, Khade B, Gera PB, Gupta S. Establishing a correlation between RIN and A(260/280) along with the multivariate evaluation of factors affecting the quality of RNA in cryopreserved cancer bio-specimen. *Cell Tissue Bank* 2019;**20**:489–99
21. Stauffer CE. A linear standard curve for the Folin Lowry determination of protein. *Anal Biochem* 1975;**69**:646–8
22. Zaret K. Micrococcal nuclease analysis of chromatin structure. *Curr Protoc Mol Biol* 2005;**21**:**21**.1
23. Khan SA, Tyagi M, Sharma AK, Barreto SG, Sirohi B, Ramadwar M, Shrikhande SV, Gupta S. Cell-type specificity of β-actin expression and its clinicopathological correlation in gastric adenocarcinoma. *World J Gastroenterol* 2014;**20**:12202–11
24. Sharma AK, Bhattacharya S, Khan SA, Khade B, Gupta S. Dynamic alteration in H3 serine 10 phosphorylation is G1-phase specific during ionization radiation induced DNA damage response in human cells. *Mutat Res* 2015;**773**:83–91
25. Wang W, Caldwell MC, Lin S, Furneaux H, Gorospe M. HuR regulates cyclin A and cyclin B1 mRNA stability during cell proliferation. *EMBO J* 2000;**19**:2340–50
26. Trojanowicz B, Dralle H, Hoang-Vu C. AUF1 and HuR: possible implications of mRNA stability in thyroid function and disorders. *Thyroid Res* 2011;**4**:S5
27. Guo YJ, Pan WW, Liu SB, Shen ZF, Xu Y, Hu LL. ERK/MAPK signalling pathway and tumorigenesis. *Exp Ther Med* 2020;**19**:1997–2007
28. Zhao X, McKillop-Smith S, Müller B. The human histone gene expression regulator HBP/SLBP is required for histone and DNA synthesis, cell cycle progression and cell proliferation in mitotic cells. *J Cell Sci* 2004;**117**:6043–51
29. Reddy D, Bhattacharya S, Shah S, Rashid M, Gupta S. DNA methylation mediated downregulation of histone H3 variant H3.3 affects cell proliferation contributing to the development of HCC. *Biochim Biophys Acta Mol Basis Dis* 2022;**1868**:166284
30. Zhang W, Poirier L, Diaz MM, Bordignon V, Clarke HJ. Maternally encoded stem-loop-binding protein is degraded in 2-cell mouse embryos by the co-ordinated activity of two separately regulated pathways. *Dev Biol* 2009;**328**:140–7
31. Brocato J, Fang L, Chervona Y, Chen D, Kiok K, Sun H, Tseng HC, Xu D, Shamy M, Jin C, Costa M. Arsenic induces polyadenylation of canonical histone mRNA by down-regulating stem-loop-binding protein gene expression. *J Biol Chem* 2014;**289**:31751–64
32. Puscheck EE, Awonuga AO, Yang Y, Jiang Z, Rappolee DA. Molecular biology of the stress response in the early embryo and its stem cells. *Adv Exp Med Biol* 2015;**843**:77–128
33. Bustaffa E, Stoccoro A, Bianchi F, Migliore L. Genotoxic and epigenetic mechanisms in arsenic carcinogenicity. *Arch Toxicol* 2014;**88**:1043–67
34. Schmidlin M, Lu M, Leuenberger SA, Stoecklin G, Mallaun M, Gross B, Gherzi R, Hess D, Hemmings BA, Moroni C. The ARE-dependent mRNA-destabilizing activity of BRF1 is regulated by protein kinase B. *EMBO J* 2004;**23**:4760–9
35. Wilson GM, Lu J, Sutphen K, Suarez Y, Sinha S, Brewer B, Villanueva-Feliciano EC, Ysla RM, Charles S, Brewer G. Phosphorylation of p40AUF1 regulates binding to A + U-rich mRNA-destabilizing elements and protein-induced changes in ribonucleoprotein structure. *J Biol Chem* 2003;**278**:33039–48
36. Wilson GM, Lu J, Sutphen K, Sun Y, Huynh Y, Brewer G. Regulation of A + U-rich element-directed mRNA turnover involving reversible phosphorylation of AUF1. *J Biol Chem* 2003;**278**:33029–38
37. Maya Miles D, Peñate X, Sanmartín Olmo T, Jourquin F, Muñozz Centeno MC, Mendoza M, Simon M-N, Chavez S, Geli V. High levels of histones promote whole-genome-duplications and trigger a Swe1(WEE1)-dependent phosphorylation of Cdc28(CDK1). *eLife* 2018;**7**:e35337
38. Harari Y, Ram Y, Kupiec M. Frequent ploidy changes in growing yeast cultures. *Curr Genet* 2018;**64**:1001–4
39. Harari Y, Ram Y, Rappoport N, Hadany L, Kupiec M. Spontaneous changes in ploidy are common in yeast. *Curr Biol* 2018;**28**:825–35
40. Vicente-Dueñas C, Hauer J, Cobaleda C, Borkhardt A, Sánchez-García I. Epigenetic priming in cancer initiation. *Trends Cancer* 2018;**4**:408–17

(Received August 22, 2022, Accepted February 9, 2023)